Simulating the Influence of Temperature on Microwave Transmissivity of Trees During Winter Observed by Spaceborne Microwave Radiometery

Qinghuan Li, Richard Kelly, Juha Lemmetyinen, and Jinmei Pan

***Abstract*—Forest transmissivity is a key parameter for understanding spaceborne and airborne observations of the Earth's land surface because not only does it influences the proportion of subcanopy upwelling microwave emission penetrating through the forest canopy, it also controls the forest thermal emission. In frozen winter conditions, our previous study has indicated that observed microwave transmissivity of trees is also strongly influenced by temperature. This follow-on study uses ground-based radiometer observations, advanced microwave scanning radiometer 2 (AMSR2) observations, and model simulation to evaluate how this temperature-transmissivity relationship affects spaceborne passive microwave (PM) snow observations. A model is developed to simulate the relationship between tree transmissivity and air temperature. The R^2 of the model is 0.85 (0.81) with a root mean square error (RMSE) of 0.03 (0.03) at the 18.7 (36.5) GHz channels, respectively. We find that this temperature-transmissivity relationship has a significant influence on the Tb of the tree, which influences both ground-based radiometer and spaceborne AMSR2 observations. The influence of the temperature-transmissivity relationship on upwelling ground emission is frequency dependent, demonstrating that the findings have implications for frequency difference based approaches for PM snow depth and snow water equivalent retrievals which observe snow-covered landscapes, including boreal forests, at air temperatures below freezing. This effect should therefore be accounted for in frequency difference or ratio approaches of snow accumulation retrievals.**

***Index Terms*—Snow, transmissivity, temperature, tree.**

I. Introduction

FOREST cover is a key land cover type in snow affected regions, especially at mid-latitudes. Trees have a strong microwave attenuation and emission capacity. Their complex structures and biophysical processes mean that the presence of forests present a major challenge to the accuracy of airborne and spaceborne passive microwave (PM) geophysical parameter observation retrievals of snow water equivalent (SWE), snow depth (SD) [1]–[4], and soil moisture [5].

The first order forest radiative transfer models are usually applied for correcting the influence of the forest on geophysical parameter retrievals [e.g., 5, 14–16]. In PM remote sensing, the forest canopy layer usually be estimated as a nonscattering, attenuating layer in the radiative transfer equation [15], [16]. Therefore, transmissivity, as the inverse value of attenuation which defines the portion of electromagnetic radiation penetrating this layer, is the key parameter. The transmissivity of trees is strongly influenced by the permittivity of the vegetation tissue [6], [7]. Vegetation water content is a key factor controlling the permittivity, with dry tissue exhibiting the lowest permittivity [8]. Under subzero temperatures (°C), the water stored in vegetation freezes as temperatures drop. Hence, the free water content decreases due to this phase change. Since at microwave frequencies the permittivity of ice (∼3) is typically lower than that of water (∼80), the overall effective permittivity of the vegetation tissue decreases. This phenomenon was observed by experiment on a small piece of corn leaf [9]. However, for natural trees in cold regions, antifreeze mechanisms can mitigate the freezing process [10], [11], [36]. Furthermore, the factors like the solar radiation can cause the thermal heterogeneous of the tree mass. For example, Mayr *et al.* [12] found that the freezing and thawing rate at the top of the tree is greater than at the trunk base. Therefore, tree water content freezing is a complex and uneven process in a natural environment. Li *et al.* [13] observed a season-long temperature-transmissivity relationship in a Scots pine tree, and found that microwave transmissivity, measured at several frequencies from 10.65 to 37 GHz, changed gradually with temperature at below-freezing conditions.

Tree transmissivity variations caused by below-freezing temperatures have a significant influence on the Tb of the tree [13], but typical transmissivity models for forest vegetation ignore this effect (e.g., [14]–[16], [33], [34]). In snow parameter retrievals, typical transmissivity models consider transmissivity as a constant value related to structural parameters, such as the forest stem volume and density (e.g., [14]–[16]) or vegetation index (e.g., [30], [31]). Therefore, for observations of cold season snow accumulation, especially SWE, a significant bias is likely

Manuscript received March 18, 2020; revised June 22, 2020; accepted August 11, 2020. Date of publication August 18, 2020; date of current version August 31, 2020. This work was supported in part by INTERACT under the European Union H2020 Grant Agreement 730938, in part by JAXA GCOM-W, and in part by Natural Sciences and Engineering Research Council Discovery under Grant RGPIN-2017-04385. *(Corresponding author: Qinghuan Li.)*

Qinghuan Li and Richard Kelly are with the Department of Geography and Environmental Management, University of Waterloo, Waterloo, ON N2L 3G1, Canada (e-mail: q97li@uwaterloo.ca; rejkelly@uwaterloo.ca).

Juha Lemmetyinen is with the Space and Earth Observation Centre, Finnish Meteorological Institute, 99600 Sodankylaä, Finland (e-mail: juha.lemmetyinen@fmi.fi).

Jinmei Pan is with the State Key Laboratory of Remote Sensing Science, Aerospace Information Research Institute,Chinese Academy of Sciences, Beijing 100101, China (e-mail: panjm1987@radi.ac.cn).

Digital Object Identifier 10.1109/JSTARS.2020.3017618

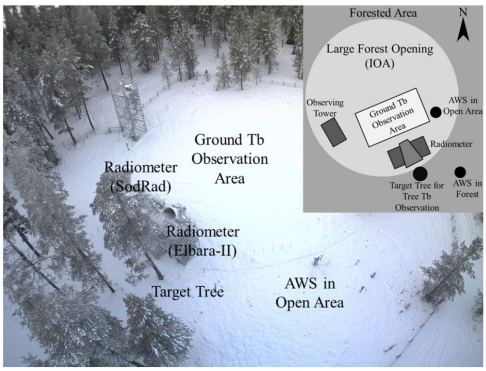

Fig. 1. Study site and the configuration of the experiment.

introduced if this temperature-transmissivity relationship is ignored. Because the influence of the temperature-transmissivity relationship on upward ground brightness temperature (Tb) is likely frequency dependent, the Tb difference (ΔTb) approaches between a low frequency Tb and a high frequency Tb for SD and SWE retrievals (e.g., 18.70 and 36.5 GHz) [17]–[19] may also be influenced. A major advantage of the Tb difference approach is that the low frequency channel (e.g., 18 GHz) can be regarded as a reference channel to mitigate the influence of temperature [17]. However, how the temperature-transmissivity relationship could influence the ΔTb is unknown.

In this study, a model to describe the tree temperature-transmissivity relationship is developed using *in-situ* field observations and measurements. Then, the potential influence of this relationship on snow parameter retrievals from space is evaluated. Section II outlines the applied methodology and data. Section III gives the main results of our study. These are further discussed in Section IV; Section V provides the Conclusion.

II. Methodology and Data

A. Study Site and the Configuration of the Experiment

This study was conducted using ground-based and satellite data collected over a site near Sodankylä, Finland (67.36 N, 26.63 E). Sodankylä typifies the landscape in the boreal forest belt. Considering an area of 791 134 ha around Sodankylä, Boreal forest covers 54.7% of the land cover in this region, and is mixed with about 75.4% pine, 14.7% spruce, and 9.8% birch [21]. Ground-based instruments were located in a forest opening, called the intensive observation area (IOA) (shown in Fig. 1). The IOA is surrounded by sparse pine forest with trees about 15 m high. The measurement setup allowed ground-based instruments to observe both the ground in the forest opening, as well as a single Scots Pine (*Pinus Sylvestris L.*) specimen from beneath the canopy [13].

The up-welling microwave Tb of the ground (Tb_{ground}), the down-welling Tb of the specimen tree ($Tb_{\downarrow\mathrm{tree}}$), and the down-welling Tb of the sky (Tb_{sky}) were observed by the Sodankylä Radiometer (SodRad) system located at the edge of the forest opening. Ancillary data were collected from adjacent automatic weather stations (AWS) located inside the forest and inside the forest opening. Fig. 1 illustrates the configuration of the study site.

B. Data Sources

1) Radiometer Observations: The SodRad radiometer system was mounted on a 4.1 m high platform located at the edge of the forest opening. It is a four-frequency dual-polarization system operating at 10.65, 18.7, 21, and 36.5 GHz channels in both horizontal (H) and vertical (V) polarizations. The bandwidths for all frequencies are 400 MHz, the absolute system stability is 1.0 K, the half-power beam width is 6.0°, and the sidelobe level is less than -30 dB [22].

The radiometer made a full azimuth-elevation scan [13]. The Tb observations were conducted daily during 11:00 to 3:00 A.M. and 11:00 to 3:00 P.M. UTC. The horizontal distance between the target tree and the radiometer was about 3 m, and the ground and the sky were scanned in the opposite direction of the tree scan. In this study, the Tb observations of the ground (Tb_{ground}), the downwelling radiation from the trees ($Tb_{\downarrow\mathrm{tree}}$), and the sky ($Tb_{\mathrm{sky}}$) at 45° elevation each day from September 5, 2016 to April 17, 2017 are used.

2) Ancillary Data Sets: The ancillary data used in the study include the air temperature (T_{air}), snow temperature (T_{snow}),SD, and soil temperature (T_{soil}). Measurements were acquired every ten min by two AWS, one in the forest and another in the forest opening. T_{air} and SD were measured in both forest and forest opening by the AWS. T_{air} was measured at the height of 2 m by a Vaisala PT100 sensor, whereas SD was measured by a Campbell Scientific SR50 acoustic sensor. T_{snow} and T_{soil} were measured by Campbell Scientific 107-L sensors in the IOA forest opening. T_{snow} was measured from 0 to 120 cm at 10 cm intervals, and T_{soil} was measured at a depth of 5 cm.

3) Satellite Observation: The satellite observed ground emission (Tb_{AMSR}) from September 1, 2016 to April 30, 2017 was obtained by the advanced microwave scanning radiometer 2 (AMSR2) [20] on-board the global change observation mission 1st-water (GCOM-W1) satellite. The descending passes were chosen with an 11:00 P.M. to 2:30 A.M. overpass time; usually one or two descending passes crossed the IOA each day. Tb_{AMSR} was extracted from the Level 1 resampling product [23]. This study used the Tb at 18.7 and 36.5 GHz in V polarization. The footprints of the Tbs at both frequencies were resampled to an 24 $\times$ 42 km ellipse (along scan $\times$ along track). AMSR2 footprints closest to the coordinates of the IOA in the were selected.

C. Model Description

1) Tree Emission Modeling: According to Mätzler [24], the downwelling emission from a tree ($Tb_{\downarrow\mathrm{tree}}$) can be approximated so that

$$Tb_{\downarrow\mathrm{tree}} = (1-\gamma-r_{\mathrm{forest}})\ T + \ \gamma Tb_{\mathrm{sky}} + \ r_{\mathrm{forest}} Tb_{\mathrm{ground}} \tag{1}$$

where γ and r_{forest} are the transmissivity and the reflectivity of the tree, respectively and T is the temperature of the tree. Because the skin temperature of the tree is very close to the air temperature [13], we regard T equals to air temperature. The first

term in (1), $(1-\gamma-r_{\rm forest})T$, represents the thermal emission from the tree, the second term ($\gamma Tb_{\rm sky}$) represents the sky Tb penetrated through the tree, and the third term ($r_{\rm forest}Tb_{\rm ground}$) represents the upwelling Tb from the ground which is reflected back down by the tree. The upwelling Tb of the tree ($Tb_{\uparrow{\rm tree}}$) can be written as

$$\begin{aligned} Tb_{\uparrow{\rm tree}} = {} & (1-\gamma-r_{\rm forest})\ T + \ \gamma Tb_{\rm ground} \\ & + \gamma r_{\rm ground}\,(1-\gamma-r_{\rm forest})\,T \\ & + r_{\rm forest}Tb_{\rm sky} + r_{ground}\gamma^2 Tb_{sky} \end{aligned} \tag{2}$$

where $(1-\gamma-r_{\rm forest})T$ is the thermal emission from the tree, $\gamma Tb_{\rm ground}$ is the upward ground Tb penetrated through the tree, $\gamma r_{\rm ground}(1-\gamma-r_{\rm forest})T$ is the downward thermal emission from the tree which is reflected up by the ground and then pass through the tree, $r_{\rm forest}Tb_{\rm sky}$ is the downward sky Tb which is reflected up by the tree, and $r_{\rm ground}\gamma^2 Tb_{\rm sky}$ is the downward sky Tb that is reflected by the ground, attenuated by the two-way transmissivity of the tree. In (1) and (2), $Tb_{\rm ground}$ and $Tb_{\rm sky}$ are obtained by the SodRad, and T is approximated using the air temperature $T_{\rm air}$ measured by the AWS. Since $r_{\rm forest}$ is typically small, considering the vegetation thus as a simple attenuating layer is a common approach in emission models [15], [25]–[27]. Therefore, we assume $r_{\rm forest}$ is 0. Following the approach developed by Mätzler, the transmissivity γ can be estimated by (3) [24]. The γ term calculated by Mätzler's approach is denoted as γ_M.

$$\gamma_M = \frac{T - Tb_{\downarrow{\rm tree}}}{T - Tb_{\rm sky}} \tag{3}$$

Considering $T_{\rm ground}$ equals $T_{\rm soil}$, the thermal equilibrium $r_{\rm ground}$ is estimated by

$$r_{\rm ground} \approx 1 - \frac{Tb_{\rm ground}}{T_{\rm ground}} \tag{4}$$

2) Empirical Model of Temperature-Transmissivity Relationship: In the work of Li *et al.* [13], a linear regression model was developed to describe the relationship between the tree transmissivity and temperature. Tree transmissivity is sensitive to subzero temperatures because subzero (degrees Celsius) temperatures progressively freeze the vegetation water content. As the temperature decreases further, less and less water content in the vegetation tissue is available to be frozen. This might explain why the transmissivity is nonlinearly related to the temperature in Fig. 2, which shows transmissivity calculated from Matzler's approach (3) as a function of tree temperature. Therefore, instead of using the linear regression model, we used the following equation to obtain a better fit to the relationship between $T_{\rm air}$ and γ_M.

$$\begin{aligned} \gamma &= 1 - \frac{(1-\gamma_0)}{1-a_\gamma T} \quad T \le 0 \\ \gamma &= \gamma_0 \quad T > 0 \end{aligned} \tag{5}$$

where a_γ is an empirical parameter, T is the air temperature (°C), and γ_0 is the tree transmissivity when $T_{\rm air} > 0$ °C. The second term of (5) ($\frac{1}{1-a_\gamma T}$) is a function used to control the curve shape of (5) by adjusting the value of $1-\gamma_0$. The value of ($\frac{1}{1-a_\gamma T}$) increases in the interval of (0, 1] with T in the interval of (-∞,0]. Therefore, the value of (5) increases in the interval of (1, γ_0] when T changes at the interval of (-∞,0]. In this study, for estimating the parameters of (5), the average γ_M calculated for $T_{\rm air} > 0$ °C is regarded as γ_0. a_γ is estimated by the least squares fitting method according to the γ_M assuming that the value of γ_0 is determined.

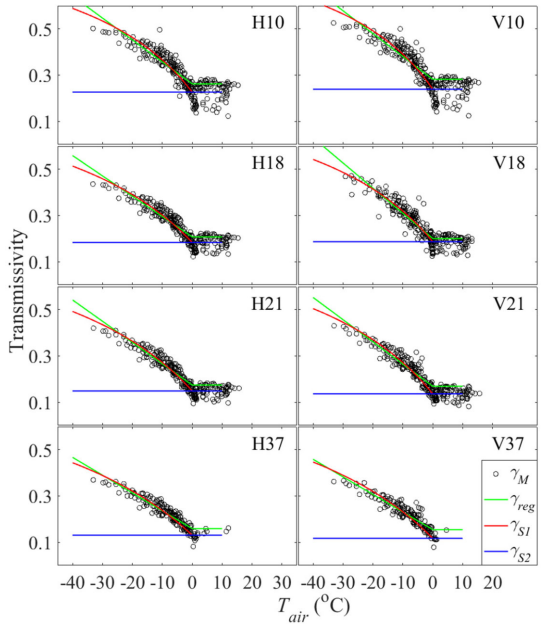

Fig. 2. Variations in γ_M with air temperature T (circle markers). The linear fit lines represent γ_{S1} (red lines), γ_{S2} (blue lines), and $\gamma_{\rm reg}$ (green lines).

D. Influence of Temperature-Transmissivity Relationship on Tree Emission and Forested Snow Scene for AMSR2 Tb Observations

To evaluate the influence of the temperature-transmissivity relationship on tree emission, the tree transmissivity γ, $Tb_{\downarrow{\rm tree}}$, $Tb_{\uparrow{\rm tree}}$, and the ΔTb of the $Tb_{\uparrow{\rm tree}}$ between 18.7 and 36.5 GHz channel in V polarization ($\Delta Tb_{\uparrow{\rm tree}}$) were simulated for two scenarios using (1), (2), and (5). In $Scenario1$, the transmissivity was calculated based on the temperature-transmissivity relationship model in (5). Accordingly, the simulated results are written as: γ_{S1}, $Tb_{\downarrow{\rm tree\_}S1}$, $Tb_{\uparrow{\rm tree\_}S1}$, and $\Delta Tb_{\uparrow{\rm tree\_}S1}$. For $Scenario2$, the temperature-transmissivity relationship is ignored, so transmissivity is considered as $\gamma = \gamma_0$ in all the temperature. Accordingly, the simulated results are written as: γ_{S2}, $Tb_{\downarrow{\rm tree\_}S2}$, $Tb_{\uparrow{\rm tree\_}S2}$, and $\Delta Tb_{\uparrow{\rm tree\_}S2}$. The difference of the simulated results between $Scenario1$ and $Scenario2$ reveals how the temperature-transmissivity relationship can influence tree emission and the ΔTb. The transmissivity estimates from the linear regression model developed by Li *et al.* ($\gamma_{\rm reg}$) [13], and the tree downwelling emission simulated by (1) based on $\gamma_{\rm reg}$ ($Tb_{\downarrow{\rm tree\_reg}}$) are also calculated. γ_{S1}, γ_{S2} and $\gamma_{\rm reg}$ are compared with γ_M while $Tb_{\downarrow{\rm tree\_}S1}$, $Tb_{\downarrow{\rm tree\_}S2}$, and $Tb_{\downarrow{\rm tree\_reg}}$ are compared with the radiometer observed $Tb_{\downarrow{\rm tree}}$.

TABLE I
ESTIMATED PARAMETERS (γ_0 AND a_γ) AND THE RMSE OF (5) AND THE LI *ET AL.*

	H10	V10	H18	V18	H21	V21	H37	V37
γ_0	0.23	0.24	0.18	0.19	0.15	0.14	0.13	0.12
a_γ	0.02	0.03	0.02	0.02	0.02	0.02	0.01	0.02
RMSE_S1 (%)	15.68	15.70	11.83	13.82	12.55	13.90	10.07	11.57
RMSE_reg (%)	21.83	22.87	16.58	16.24	19.11	23.60	13.65	14.43

To evaluate the influence of the temperature-transmissivity relationship on spaceborne PM observations, the Tb at the AMSR scale is simulated ($Tb_{\mathrm{AMSR\_sim}}$) in $Scenario1$ and $Scenario2$ (Tb_{AMSR_S1} and Tb_{AMSR_S2}) based on the value of $Tb_{\uparrow \mathrm{tree}\_S1}$ and $Tb_{\uparrow \mathrm{tree}\_S2}$ by the (6). Tb_{AMSR_S1} and Tb_{AMSR_S2} are compared with the spaceborne observed Tb_{AMSR}

$$Tb_{\mathrm{AMSR\_sim}} = fTb_{\uparrow \mathrm{tree}} + (1-f)\,Tb_{\mathrm{ground}} \qquad (6)$$

where f is the forest fraction. Accordingly, the Tb difference of the 18.7 and 36.5 GHz channels in V polarization (ΔTb) at the AMSR scale in $Scenario1$ and $Scenario2$ ($\Delta Tb_{\mathrm{AMSR\_S1}}$ and ΔTb_{AMSR_S2}) are calculated based on the value of Tb_{AMSR_S1} and Tb_{AMSR_S2}. The ΔTb of the Tb_{AMSR} ($\Delta Tb_{\mathrm{AMSR}}$) is compared with $\Delta Tb_{\mathrm{AMSR}\_S1}$ and $\Delta Tb_{\mathrm{AMSR}\_S2}$. Because the algorithms for global SWE and SD estimation typically rely on the sensitivity of ΔTb to SWE and SD (e.g., [17]–[19]), this comparison reveals how the temperature- transmissivity relationship can influence the PM spaceborne SWE and SD retrieval.

III. RESULTS

A. Relationship Between Tree Transmissivity and Air Temperature

Fig. 2 shows the air temperature - transmissivity (γ_M) relationship based on the model from (5). Three different statistical model fits are superimposed on the data and are shown as γ_{S1}, γ_{S2}, γ_{reg}. γ_{S1} is the transmissivity calculated from $Scenario1$, which considers the temperature- transmissivity relationship; while γ_{S2} is the transmissivity calculated from $Scenario2$, which regards transmissivity as a constant; and γ_{reg} is the transmissivity estimated by the linear regression model developed by Li *et al.* [13].

According to γ_M in Fig. 2, the transmissivity of the tree increases as air temperature decreases, while the transmissivity is insensitive to air temperatures higher than 0 °C. Fig. 2 indicates that the model that uses the air temperature adjustment (γ_{S1}) fits well with the observed results. The comparison between γ_{S1} (temperature sensitive) and γ_{S2} (temperature insensitive) indicates that the temperature is a major factor causing the tree transmissivity variations of up to 0.3 under subzero temperatures. In addition, γ_{S1} has a better match with the model estimates of γ_M than γ_{reg}, especially when T_{air} under −20 °C.

Table I presents the estimated value of parameters γ_0 and a_γ in (5) for all investigated channels. RMSE_S1 is the root mean square error presented as the percentage (RMSE) of γ_{S1} againstγ_M. RMSE_reg is the RMSE of γ_{reg} against γ_M. According to Table I, RMSE_S1 is lower than RMSE_reg, which indicates that the estimated results of (5) provided a better fit to γ_M than the linear regression model developed by Li *et al.* [13].

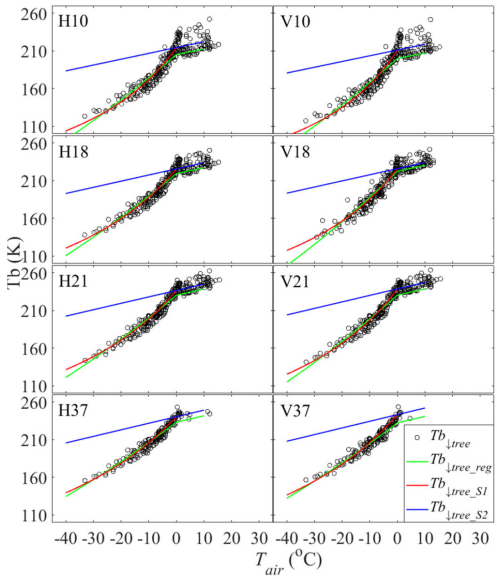

Fig. 3. Variations in $Tb_{\downarrow \mathrm{tree}}$ with air temperature observed by the SodRad radiometer (circle markers). The different lines show simulations of Tb in $Tb_{\downarrow \mathrm{tree}\_S1}$ (red line), $Tb_{\downarrow \mathrm{tree}\_S2}$ (blue lines), and $Tb_{\downarrow \mathrm{tree\_reg}}$ (green lines).

TABLE II
RMSE OF SIMULATED SCENARIO S1 (RMSE_TB_S1) AND THE LIEAR RELATION BY LI *ET AL.* (RMSE_TB_REG) AGAINST OBSERVED $Tb_{\downarrow \mathrm{tree}}$

	H10	V10	H18	V18	H21	V21	H37	V37
RMSE_Tb_S1 (%)	4.39	4.85	3.04	3.45	2.72	2.74	2.35	2.66
RMSE_Tb_reg (%)	5.27	5.97	3.71	3.89	3.45	3.59	2.65	2.66

According to Table I, RMSE_S1 is lower than RMSE_reg, which indicates that the estimated results of (5) provided a better fit to γ_M than the linear regression model developed by Li *et al.* [13].

Having determined that tree transmissivity is strongly controlled by the air temperature, it is possible to estimate $Tb_{\downarrow \mathrm{tree}}$ using (1) and (5). Fig. 3 shows the radiometer observed $Tb_{\downarrow \mathrm{tree}}$ and the model simulations of the two model scenarios when corrected for air temperature, $Tb_{\downarrow \mathrm{tree}\_S1}$, and when air temperature is ignored, $Tb_{\downarrow \mathrm{tree}\_S2}$. The $Tb_{\downarrow \mathrm{tree\_reg}}$ is the Tb of the tree simulated by (1) with γ_{reg} [13].

Table II gives the RMSE of the simulated $Tb_{\downarrow \mathrm{tree}\_S1}$ (RMSE_Tb_S1) and $Tb_{\downarrow \mathrm{tree\_reg}}$ (RMSE_Tb_reg) against observed $Tb_{\downarrow \mathrm{tree}}$.

According to Fig. 3 and Table II, the tree emission models [(1) and (2)] and the temperature- transmissivity relationship model (5) explained the variation of the radiometer-observed tree emission in this experiment. $Tb_{\downarrow \mathrm{tree}}$ responds to the air temperature as temperatures fall below 0 °C. Without the temperature-transmissivity correction ($Scenario2$), estimated $Tb_{\downarrow \mathrm{tree}\_S2}$ decreases linearly with air temperature. The difference between the two scenario models increases to more than 30 K as temperature drops to −20 °C indicating a significant bias. $Tb_{\downarrow \mathrm{tree}\_S1}$ has a better match with $Tb_{\downarrow \mathrm{tree}}$ than $Tb_{\downarrow \mathrm{tree\_reg}}$, especially when T_{air} under −20 °C, which indicates that the (5) is a better option to be applied than the linear regression model developed by Li *et al.* [13] in this case study.

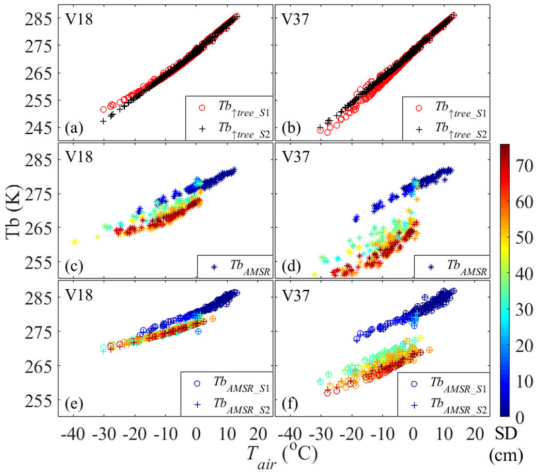

Fig. 4. Simulated $Tb_{\uparrow \mathrm{tree}\_S1}$ (red circle markers) and $Tb_{\uparrow \mathrm{tree}\_S2}$ (black cross markers) in (a) and (b). Observed Tb_{AMSR} (star marker with blue-green-yellow colors) in (c) and (d). Simulated Tb_{AMSR_S1} (circle makers with blue-green-yellow colors) and Tb_{AMSR_S2} (star makers with blue-green-yellow colors) in (e) and (f). Blue-green-yellow star markers represent AMSR2 Tbs for different snow depths (blue-green-yellow scale) in the forest opening.

B. Evaluation of Temperature Influences on Transmissivity Affecting Tb Emissions: Implications for PM Snow Retrievals

The ΔTb between 18.7 and 36.5 GHz channels in V polarization is often used in snow parameter retrievals. Therefore, in this section, we discuss the influence of the temperature-transmissivity relationship on these two channels. The discussion relating to other channels can be found in [35].

In Fig. 4, $Tb_{\uparrow \mathrm{tree}\_S1}$, $Tb_{\uparrow \mathrm{tree}\_S2}$ are presented in (a) and (b); the Tb_{AMSR} is presented in (c) and (d); Tb_{AMSR_S1} and Tb_{AMSR_S2} are presented in (e) and (f). The Blue-Green-Yellow scale bar and the colors of Tb_{AMSR}, Tb_{AMSR_S1}, and Tb_{AMSR_S2} markers represent the snow depth (a warmer color represents a thicker snow depth).

According to (a) and (b) in Fig. 4, the Tbs in both $Tb_{\uparrow \mathrm{tree}\_S1}$ and $Tb_{\uparrow \mathrm{tree}\_S2}$ decrease with a decreasing T_{air}. However, the relationship between $Tb_{\uparrow \mathrm{tree}\_S2}$ and T_{air} maintains a relatively consistent gradient from low frequency (18.7 GHz) to high frequency (36.5 GHz) estimates, while for $Tb_{\uparrow \mathrm{tree}\_S1}$ the gradients of these relationships decrease from high frequency to low frequency indicating a decreased sensitivity to T_{air} at the lower frequency Tb observations (also see Fig. 5 in [35] for 10.65 and 21 GHz). The difference between $Tb_{\uparrow \mathrm{tree}\_S1}$ and $Tb_{\uparrow \mathrm{tree}\_S2}$ increases with a decreasing T_{air}. This result indicates that the influence of the temperature -transmissivity relationship on upwelling tree emission is frequency dependent.

The pattern evident in Fig. 4(a) and (b) can also be seen in the comparison between Tb_{AMSR_S1} and Tb_{AMSR_S2} in Fig. 4(e) and (f). However, only about 54.7% of the AMSR2 observation footprint is covered by forest, and outside the forest, most of the land inside the footprint is a snow-covered ground during winter. Therefore, the Tbs in AMSR2 footprint are less influenced by the temperature-transmissivity relationship, and are more sensitive to the snow depth. It is very important to notice that the influence of the temperature-transmissivity relationship on Tbs is more obvious for thicker snow depth, especially when the snow depth

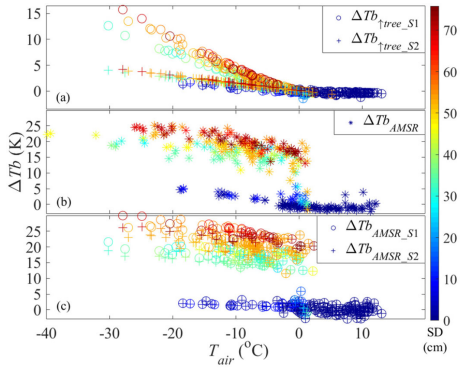

Fig. 5. Simulations of $\Delta Tb_{\uparrow \mathrm{tree}\_S1}$ (circle markers) and $\Delta Tb_{\uparrow \mathrm{tree}\_S2}$ (cross markers) in (a), Observed $\Delta Tb_{\mathrm{AMSR}}$ (star markers) in (b), and simulated $\Delta Tb_{\mathrm{AMSR}\_S1}$ (circle markers) and $\Delta Tb_{\mathrm{AMSR}\_S2}$ (cross markers) in (c). Colors of the markers represent snow depths (blue-green-red scale) in the forest opening.

is greater than 40 cm. This phenomenon will be discussed in the discussion section.

In Fig. 4(c) and (d), Tb_{AMSR} is presented. Tb_{AMSR} and Tb_{AMSR_S1} were obtained from a very different sources. Tb_{AMSR_S1} is a model simulation result based on the Tbs observed by an upwelling ground-based radiometer from a single tree while Tb_{AMSR} is a direct observation of the site from a spaceborne radiometer. However, although the overall value of Tb_{AMSR} is slightly lower than the model simulated Tb_{AMSR_S1}, Tb_{AMSR} has a similar behavior to T_{air} and snow depth as $Tb_{\uparrow \mathrm{tree}\_S1}$, which verifies the appropriateness of the Tb of the tree emission representation developed in this study.

Since the influence of the temperature-transmissivity relationship on upwelling tree emission is frequency dependent, the ΔTb is also influenced by this relationship. In Fig. 5, $\Delta Tb_{\uparrow \mathrm{tree}\_S1}$ and $\Delta Tb_{\uparrow \mathrm{tree}\_S2}$ are shown in (a), $\Delta Tb_{\mathrm{AMSR}}$ in (b) and $\Delta Tb_{\mathrm{AMSR}\_S1}$ and $\Delta Tb_{\mathrm{AMSR}\_S2}$ in (c).

Fig. 5(a) and (c) shows that when $T_{\mathrm{air}} < 0$ °C, the sensitivity of $\Delta Tb_{\uparrow \mathrm{tree}\_S1}$ and $\Delta Tb_{\mathrm{AMSR}\_S1}$ to the snow depth increases as T_{air} decreases, and that $\Delta Tb_{\uparrow \mathrm{tree}\_S1}$ and $\Delta Tb_{\mathrm{AMSR}\_S1}$ have a negative correlation with T_{air}. However, the sensitivity of $\Delta Tb_{\uparrow tree\_S2}$ and ΔTb_{AMSR_S2} to the snow depth is not influenced by T_{air}, and $\Delta Tb_{\uparrow \mathrm{tree}\_S2}$ and $\Delta Tb_{\mathrm{AMSR}\_S2}$ are almost insensitive to T_{air}. $\Delta Tb_{\mathrm{AMSR}}$ in (b) has a similar behavior as $\Delta Tb_{\uparrow \mathrm{tree}\_S1}$, and shows a high similarity with $\Delta Tb_{\mathrm{AMSR}\_S1}$, which indicates that although the observe area had only 54.7% forest coverage with a relatively low stem volume typical for Northern latitudes (∼50–70 m^3/ha), the temperature-transmissivity relationship has a similar influence on $\Delta Tb_{\mathrm{AMSR}}$. According to (a) and (c), the difference between $Scenario1$ and $Scenario2$ increases as T_{air} decreases. Below -30 °C, the difference between $\Delta Tb_{\uparrow \mathrm{tree}\_S1}$ and $\Delta Tb_{\uparrow \mathrm{tree}\_S1}$ is about 10 K, and the difference between $\Delta Tb_{\mathrm{AMSR}\_S1}$ and $\Delta Tb_{\mathrm{AMSR}\_S2}$ is more than 5 K. As in Fig. 4, the influence of temperature-transmissivity relationship on Tb difference is also more obvious for larger snow depths, especially when the snow depth is greater than 40 cm and is discussed below.

The Pearson correlation coefficient between ΔTb and T_{air} under $T_{\mathrm{air}} \leq 0$ °C is presented in Table III. The significance

TABLE III
CORRELATION TEST OF ΔTb AND $T_{\rm air}$

	Correlation coefficient	Significance level	Obs
ΔTb_{AMSR}	-0.39	**	152
ΔTb_{AMSR_S1}	-0.28	**	139
ΔTb_{AMSR_S2}	-0.16	-	139

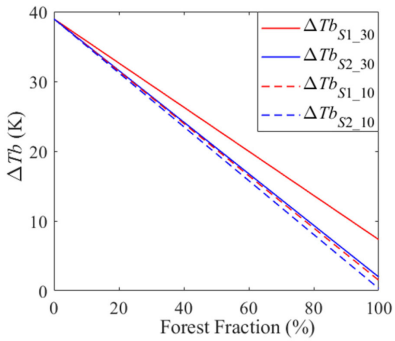

Fig. 6. Simulation of the forest fraction and the ΔTb between 18.7 and 36.5 GHz channels in V polarization for ground snow depth at 40 cm. ΔTb_{S1_10} and ΔTb_{S1_30} are the simulations in $Scenario1$ for air temperatures of -10 °C and -30 °C, respectively, and ΔTb_{S2_10} and ΔTb_{S2_30} are the simulations in $Scenario2$ for air temperatures of -10 °C and -30 °C, respectively.

notation "-" indicates that a correlation is not significant (p-value $>$ 0.05), which means that the influence of $T_{\rm air}$ on ΔTb is insignificant. while the notation "$*$" denotes a significant correlation (p-value $\leq$ 0.05) with "$**$" indicating a very high significant correlation (p-value $\leq$ 0.01). Obs means the number of the observations. According to Table II, the correlation of $\Delta Tb_{\rm AMSR}$ and $\Delta Tb_{\rm AMSR\_S1}$ to $T_{\rm air}$ is significant, while the correlation between $\Delta Tb_{\rm AMSR\_S2}$ and $T_{\rm air}$ is not significant. This result coincides with the result in Fig 5, which is the temperature-transmissivity relationship can significantly influence the ΔTb in both ground and spaceborne observations.

The Pearson correlation coefficient between ΔTb and $T_{\rm air}$ for $T_{\rm air} \leq 0$ °C is presented in Table III. The significance notation "-" indicates that a correlation is not significant (p-value $>$ 0.05), meaning that the influence of $T_{\rm air}$ on ΔTb is insignificant. while the notation "$*$" denotes a significant correlation (p-value $\leq$ 0.05) with "$**$" indicating a very high significant correlation (p-value $\leq$ 0.01). Obs means the number of the observations. According to Table II, the correlation of $\Delta Tb_{\rm AMSR}$ and $\Delta Tb_{\rm AMSR\_S1}$ to $T_{\rm air}$ is significant, while the correlation between $\Delta Tb_{\rm AMSR\_S2}$ and $T_{\rm air}$ is not significant. This result coincides with the result in Fig 5, which is the temperature-transmissivity relationship can significantly influence the ΔTb in both ground and spaceborne observations.

To demonstrate how the temperature-transmissivity relationship influences the ΔTb (18.7 and 36.5 GHz channels in V polarization) under different forest fractions, a simulation of the ΔTb and the forest fraction is presented in Fig. 6. The simulation is for ground snow depth of 40 cm, and air temperatures of -10 °C and -30 °C for a range of forest fractions (0–100%). From direct radiometer observations of the ground (no forest), the ground Tbs at 18.7 GHz and 36.5 GHz V polarization are 251.6 K and 212.7 K, respectively for the 40 cm deep snow. Using (2), (5), and (6), the ΔTbs are calculated for $Scenario1$ (the temperature-transmissivity relationship is considered) and for $Scenario2$ (the temperature-transmissivity relationship is ignored). Fig. 6 shows that the difference between $Scenario1$ and $Scenario2$ increases as the forest fraction increases. The temperature-transmissivity relationship has a stronger influence on ΔTb at the lower temperature (-30 °C).

IV. DISCUSSION

A. Relationship Between the Air Temperature and Tree Transmissivity

As air temperature decreases below the freezing mark, the water content of the vegetation tissue progressively freezes, resulting in an overall decrease of permittivity. This effect increases the transmissivity of the tree at microwave frequencies [13]. However, no study to date has attempted to model this behavior. From our study driven by Fig. 2, air temperature can be a key factor influencing tree transmissivity under subzero temperatures. According to Fig. 2 and Table I, the model developed in this article effectively described the temperature-transmissivity relation for a sample tree. The implications of this effect were explored further in Figs. 3 and 4, which demonstrate that this temperature-transmissivity relationship significantly influences the downward and upward tree emission under subzero temperature. Therefore, to ignore the temperature-transmissivity relationship during the tree emission modeling could lead to a significant bias in estimated Tb. As Fig. 3 shows, the difference between $Tb_{\downarrow {\rm tree\_S1}}$ and $Tb_{\downarrow {\rm tree\_S2}}$ is larger than 30 K in -30 °C temperatures. Hence, we suggest that this temperature-transmissivity relationship under subzero temperature should be accounted for in the retrievals of scene paramaters under forested landscapes.

As shown in Figs. 2 and 3, with decreasing temperature, the freezing process tends cease because less and less free liquid water remains in the vegetation tissue having been frozen. This phenomenon influences tree emission, ignored in the work of [13] but introduced in this study as a new function (5). However, the biophysical process controlling the water content of the tree under subzero temperature is complicated [10] and [11], and the permittivity of the vegetation tissue is influenced by its location (e.g., branches, trunks, or leaves) as well as tree species [32]. In addition to the freezing and thawing, other factors, such as drought and xylem embolism can influence the water content of the tree during winter [28]. In this study, based on the strong fit between the models simulated results and the observed results, using the function $\frac{1}{1-a_\gamma * T}$ to control the curve line shape of (5) provided a better fit than other types of functions. However, the curve line shape of temperature-transmissivity relationship may vary for different tree species or environmental conditions, for example, the exponential or logarithmic functions may work better in other experiments. Hence, the curve function may need to be adjusted.

Since our experiment only focused on one target tree, the developed model representation should be tested in more situations in future studies. Furthermore, a comprehensive experiment evaluating tree winter biophysical dynamics concurrent with microwave observations could help us to develop a better characterization of the tree emission mechanisms.

B. Influence of the Temperature-Transmissivity Relationship on Tree Emission and on the AMSR2 Observation in Forested Regions

The comparison between the simulated Tbs in $Scenario1$ and $Scenario2$ indicates that the temperature-transmissivity relationship influences $Tb_{\downarrow\mathrm{tree}}$ (Fig. 3), $Tb_{\uparrow\mathrm{tree}}$ (Fig. 4), and $\Delta Tb_{\uparrow\mathrm{tree}}$ (Fig. 5). After comparing AMSR2 observations with $Scenario1$ and $Scenario2$, the influence of the temperature-transmissivity relationship on spaceborne observations can be observed. For $Tb_{\downarrow\mathrm{tree}}$, the thermal emission $(1-\gamma-r_{\mathrm{forest}})T$ is its major component. At progressively lower subzero temperatures, the corresponding increase in tree transmissivity reduces the tree emissivity. Because the tree emissivity has a positive correlation with air temperature, the sensitivity of $Tb_{\downarrow\mathrm{tree}}$ to air temperature is enhanced by the influence of temperature-transmissivity relationship. In $Tb_{\uparrow\mathrm{tree}}$, the tree thermal emission $(1-\gamma-r_{\mathrm{forest}})T$ and the ground emission penetrated through the tree canopy $\gamma Tb_{\mathrm{ground}}$ are the two major elements. As γ decreases, the tree thermal emission increases, while the ground emission penetrated through the tree canopy decreases, and vice versa. Therefore, in $Tb_{\uparrow\mathrm{tree}}$, the temperature-transmissivity relationship influences both tree thermal emission and ground emission penetrated through the tree canopy, and these two effects tend to cancel each other out. When Tb_{ground} is relatively high, the influence of temperature-transmissivity relationship on ground emission penetrated through the tree canopy dominates. In this situation, the sensitivity of $Tb_{\uparrow\mathrm{tree}}$ to air temperature decreases (18.7 GHz in Fig. 4). While when Tb_{ground} is relatively low, the influence of temperature-transmissivity relationship on tree thermal emission dominates, so the sensitivity of $Tb_{\uparrow\mathrm{tree}}$ to air temperature increases (e.g., 36.5 GHz in Fig. 4). Over snow-covered ground, Tb_{ground} low-frequency channels have greater Tbs than high frequency Tbs because the lower frequency channels have a higher-penetration capacity to snowpack than high-frequency channels. Therefore, the influence of the temperature-transmissivity relationship on $Tb_{\uparrow\mathrm{tree}}$ is frequency dependent when the ground is covered by snow. Because the depth of the snowpack is the major reason for the Tb_{ground} difference between the 18.7 and 36.5 GHz channels, the influence of temperature-transmissivity relationship on upwelling tree emission is more obvious when the ground snow is deeper, as shown in Figs. 5 and 6.

As Fig. 4 shows, the temperature-transmissivity relationship decreases the sensitivity of $Tb_{\uparrow\mathrm{tree}}$ to the air temperature at 18.7 GHz, but slightly increases sensitivity at 37 GHz. As a consequence, $\Delta Tb_{\uparrow\mathrm{tree}}$ is influenced by the temperature-transmissivity relationship. As Fig. 5 shows, comparing the simulated results in $Scenario1$ (considering the influence of temperature-transmissivity relationship) with the one in $Scenario2$ (ignoring the influence of temperature-transmissivity relationship), the sensitivity of $\Delta Tb_{\uparrow\mathrm{tree\_}S1}$ to snow depth increases as air temperature decreases. As previously described the difference between $\Delta Tb_{\uparrow\mathrm{tree\_}S1}$ and $\Delta Tb_{\uparrow\mathrm{tree\_}S2}$ is about 10 K in minus 30 °C. In the frequency difference algorithm developed by Chang *et al.* [29], 10 K Tb difference change translates to a 16 cm SD variation.

As is evident from Figs. 4 and 5, Tb_{AMSR} and $\Delta Tb_{\mathrm{AMSR}}$ show similar behavior as $Tb_{\uparrow\mathrm{tree\_}S1}$ and $\Delta Tb_{\uparrow\mathrm{tree\_}S1}$ with air temperature variations. This result indicates that both Tb_{AMSR} and $\Delta Tb_{\mathrm{AMSR}}$ are influenced by the temperature-transmissivity correlation. Hence, the influence of temperature-transmissivity relationship cannot be ignored in spaceborne PM observations.

One of the major purposes to introduce the low frequency channel in frequency difference algorithms is to mitigate the influence of varying physical temperature [17]. The results of this article indicate that this approach cannot reduce completely the influence of the temperature-transmissivity relationship from the forest vegetation. The $\Delta Tb_{\mathrm{AMSR}}$ variation caused by temperature change has the risk to be regarded as variations in SD and SWE in current frequency difference algorithms. Therefore, this temperature-transmissivity relationship should not be ignored by PM snow retrieval algorithms in forested regions. Since different types of forest should be considered during the retrievals, a new physical model taking into account of both variation in forest biomass and temperature-induced changes in transmissivity should be developed in future work.

V. Conclusion

Tree and by extension forest transmissivity is strongly influenced by air temperature under subzero conditions. As this study shows, transmissivity and vary by up to 0.3 ($\sim$30% of the total transmissivity range) for a tree specimen when the physical temperature decreases from 0 to -30 °C. The air temperature-transmissivity relationship significantly influences the Tb of the tree, and this influence was observed by both ground-based and spaceborne radiometer observations. The temperature-transmissivity relationship could further influence spaceborne PM snow retrieval algorithms because $\Delta Tb_{\mathrm{AMSR}}$ has a negative correlation with air temperature under subzero temperatures. Unless corrected for, this correlation between $\Delta Tb_{\mathrm{AMSR}}$ and air temperature likely will cause spaceborne PM frequency difference snow retrieval algorithms to be biased. Therefore, in this study, a model to represent the temperature-transmissivity relationship was developed. We suggest that this temperature-transmissivity relationship should be further developed to cover different vegetation conditions, and considered by PM snow retrieval algorithms.

Acknowledgment

The ground measured radiometer data and ancillary data were provided by the FMI Arctic Research Centre, the GCOM-W1 AMSR2 level 1R Tb product was provided by JAXA, and MODIS MOD44b Version 6 Vegetation Continuous Field product data were provided by NASA EOSDIS Land Processes DAAC.

REFERENCES

[1] J. L. Foster, A. T. Chang, D. K. Hall, and A. Rango, "Derivation of snow water equivalent in boreal forests using microwave radiometry," *Arctic*, vol. 44, no. 5, pp. 147–152, Jan. 1991.

[2] A. T. Chang, J. L. Foster, and D. K. Hall, "Effects of forest on the snow parameters derived from microwave measurements during the BOREAS winter field campaign," *Hydrol. Processes*, vol. 10, no. 12, pp. 1565–1574, Dec. 1996.

[3] C. Derksen, "The contribution of AMSR-E 18.7 and 10.7 GHz measurements to improved boreal forest snow water equivalent retrievals," *Remote Sens. Environ.*, vol. 112, no. 5, pp. 2701–2710, May 2008.

[4] B. J. Vander, M. T. Durand, S. A. Margulis, E. J. Kim, and N. P. Molotch, "The effect of spatial variability on the sensitivity of passive microwave measurements to snow water equivalent," *Remote Sens. Environ.*, vol. 136, pp. 163–179, Sep. 2013.

[5] T. J. Jackson and T. J. Schmugge, "Vegetation effect on the microwave emission of soils," *Remote Sens. Environ.*, vol. 36, no. 3, pp. 203–212, Jun. 1991.

[6] P. Ferrazzoli and L. Guerriero, "Passive microwave remote sensing of forests: A model investigation," *IEEE Trans. Geosci. Remote Sens.*, vol. 34, no. 2, pp. 433–443, Mar 1996.

[7] H. Huang, L. Tsang, E. Njoku, A. Colliander, T. Liao, and K. Ding, "Propagation and scattering by a layer of randomly distributed dielectric cylinders using Monte Carlo simulations of 3D Maxwell equations with applications in microwave interactions with vegetation," *IEEE Access*, vol. 5, pp. 11985–12003, 2017.

[8] F. T. Ulaby and R. P. Jedlicka, "Microwave dielectric properties of plant materials," *IEEE Trans. Geosci. Remote Sens.*, vol. 22, no. 4, pp. 406–415, Jul. 1984.

[9] M. A. El-Rayes and F. T. Ulaby., "Microwave dielectric spectrum of vegetation-part I: Experimental observations," *IEEE Trans. Geosci. Remote Sens.*, vol. GE-25, no. 5, pp. 541–549, Sep. 1987.

[10] J. Levitt, "An overview of freezing injury and survival, and its interrelationships to other stresses," in *Plant Cold Hardiness and Freezing Stress* San Francisco, CA, USA: Academic, 1987, pp. 3–16.

[11] A. Sakai, "Comparative study on freezing resistance of conifers with special reference to cold adaptation and its evolutive aspects," *Can. J. Botany*, vol. 61, no. 9, pp. 2323–2332, 1983.

[12] S. Mayr, G. Wieser, and H. Bauer, "Xylem temperatures during winter in conifers at the alpine timberline," *Agricultural Forest Meteorol.*, vol. 137, no. 1/2, pp. 81–88, Mar. 2006.

[13] Q. Li *et al.*, "The influence of thermal properties and canopy-intercepted snow on passive microwave transmissivity of a scots pine," *IEEE Trans. Geosci. Remote Sens.*, vol. 57, no. 8, pp. 5424–5433, Mar. 2019.

[14] N. Kruopis, "Passive microwave measurements of snow-covered forest areas in EMAC'95," *IEEE Trans. Geosci. Remote Sens.*, vol. 37, no. 6, pp. 2699–2705, Nov. 1999.

[15] A. Langlois, A. Royer, F. Dupont, A. Roy, K. Goita, and G. Picard, "Improved corrections of forest effects on passive microwave satellite remote sensing of snow over boreal and subarctic regions," *IEEE Trans. Geosci. Remote Sens.*, vol. 49, no. 10, pp. 3824–3837, Oct. 2011.

[16] A. Roy, A. Royer, J. Wigneron, A. Langlois, J. Bergeron, and P. Cliche, "A simple parameterization for a boreal forest radiative transfer model at microwave frequencies," *Remote Sens. Environ.*, vol. 124, pp. 371–383, Sep. 2012.

[17] R. Kelly, A. Chang, L. Tsang, and J. Foster, "A prototype AMSR-E global snow area and snow depth algorithm," *IEEE Trans. Geosci Remote Sens.*, vol. 41, no. 2, pp. 230–242, Feb. 2003.

[18] R. Kelly, "The AMSR-E snow depth algorithm: Description and initial results," *J. Remote Sens. Soc. Jpn.*, vol. 29, no. 1, pp. 307–317, Jan. 2009.

[19] K. Luojus *et al.*, "*GlobSnow-2 Product User Guide Version 1.0*," ESA, Paris, France, 2013, [Online]. Available: http://www.globsnow.info/se/GlobSnow2_SE_SWE_Product_User_Guide_v1_r1.pdf

[20] A. Okuyama and K. Imaoka, "Intercalibration of advanced microwave scanning radiometer-2 (AMSR2) brightness temperature," *IEEE Trans. Geosci. Remote Sens.*, vol. 53, no. 8, pp. 4568–4577, Mar. 2015.

[21] E. Tomppo, M. Katila, K. Mäkisara, and J. Peräsaari, "*The Multi-source national forest inventory of Finland — methods and results* ," Finnish Forest Res. Inst., Vantaa, Finland, 2011, [Online]. Available: http://www.metla.fi/julkaisut/workingpapers/2014/mwp319.htm

[22] J. Lemmetyinen *et al.*, "Nordic snow radar experiment," *Geosci. Instrum. Methods Data Syst. Discussion*, vol. 5, no. 2, pp. 1–23, Sep. 2016.

[23] T. Maeda, Y. Taniguchi, and K. Imaoka, "GCOM-W1 AMSR2 Level 1R product: Dataset of brightness temperature modified using the antenna pattern matching technique," *IEEE Trans. Geosci. Remote Sens.*, vol. 54, no. 2, pp. 770–782, Sep. 2016.

[24] C. Mätzler, "Microwave transmissivity of a forest canopy: Experiments made with a beech," *Remote Sens. Environ.*, vol. 48, no. 2, pp. 172–180, Mar. 1994.

[25] E. Njoku and D. Entekhabi, "Passive microwave remote sensing of soil moisture," *J. Hydrol.*, vol. 184, pp. 101–129, Oct. 1996.

[26] J. Pulliainen and J. Grandel, "HUT snow emission model and its applicability to snow water equivalent retrieval," *IEEE Trans. Geosci Remote Sens.*, vol. 37, no. 3I, pp. 1378–1390, May 1999.

[27] M. Takala *et al.*, "Estimating northern hemisphere snow water equivalent for climate research through assimilation of space-borne radiometer data and ground-based measurements," *Remote Sens. Environ.*, vol. 115, no. 12, pp. 3517–3529, 2011.

[28] S. Mayr, M. Wolfschwenger, and H. Bauer, "Winter-drought induced embolism in Norway spruce (Picea abies) at the Alpine timberline," *Physiologia Plantarum*, vol. 115, pp. 74–80, May 2002.

[29] A. Chang, J. Foster, and D. Hall, "Nimbus-7 SMMR derived global snow cover parameters," *Ann. Glaciol.*, vol. 9, pp. 39–44, 1987.

[30] Q. Li and R. Kelly, "Correcting satellite passive microwave brightness temperatures in forested landscapes using satellite visible reflectance estimates of forest transmissivity," *IEEE J. Sel. Topic Appl. Earth Observ. Remote Sens.*, vol. 10, no. 9, pp. 3874–3883, 2017.

[31] R. Cao *et al.*, "A simple method to improve the quality of NDVI time-series data by integrating spatiotemporal information with the Savitzky-Golay filter." *Remote Sens. Environ.*, vol. 217, pp. 244–257, 2018,.

[32] A. Franchois *et al.*, "Microwave permittivity measurements of two conifers," *IEEE Trans. Geosci. Remote Sens.*, vol. 36, no. 5, pp. 1384–1395, Sep. 1998.

[33] M. Parde, K. Goita, A. Royer, and F. Vachon, "Boreal forest transmissivity in the microwave domain using ground-based measurements," *IEEE Geosci. Remote Sens.*, vol. 2, no. 2, pp. 169–171, Apr. 2005.

[34] E. Santi, S. Paloscia, P. Pampaloni, and S. Pettinato. "Ground-based microwave investigations of forest plots in Italy," *IEEE Trans. Geosci. Remote Sens.*, vol. 47, no. 9, pp. 3016–3025, Sep. 2009.

[35] Q. Li, "The influence of winter time boreal forest tree transmissivity on tree emission and passive microwave snow observations," Ph.D. dissertation, Univ. Waterloo, Waterloo, ON, Canada, 2019.

[36] X. Kou, L. Chai, L. Jiang, S. Zhao, and S. Yan, "Modeling of the permittivity of holly leaves in frozen environments," *IEEE Trans. Geosci. Remote Sens.*, vol. 53, no. 11, pp. 6048–6057, Nov. 2015.

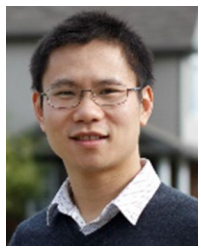

Qinghuan Li received the Ph.D. degree in geography from the University of Waterloo, Waterloo, ON, Canada, in 2019.

He is currently working at Postdoctoral fellowship with the Department of Geography and Environmental Management, University of Waterloo. His research focuses on the snow mapping with PM remote sensing in the forested region.

Richard Kelly received the Ph.D. degree in geography from the University of Bristol, Bristol, U.K., in 1995.

He is a Professor of physical geography with the University of Waterloo, Waterloo, ON, Canada. He has held academic and research positions with the University of London and NASA GSFC. He is the PI for JAXA's AMSR2 standard snow depth product and has extensive experience in satellite microwave analysis of the cryosphere and field experiments using ground based microwave systems in cold season environments. His research interests are concerned with the microwave remote sensing of snow and ice.

Dr. Kelly is a member of the AGU, IEEE Geoscience and Remote Sensing Society, and was the President of the Eastern Snow Conference.

Juha Lemmetyinen received the D.Sc. (Tech) degree in electrical engineering from Aalto University [former Helsinki University of Technology, TKK], Espoo, Finland, in 2012.

From 2004 to 2008, he was a Researcher with the TKK Laboratory of Space Technology, Department of Radio Science and Engineering, where he specialized in radiometer calibration techniques and remote sensing. From 2009 to 2013 was a scientist with the Arctic Research Unit, Finnish Meteorological Institute, Helsinki, Finland. Since 2014, he has acted as head of group at FMI for research on cryosphere processes. His current research interests include applications of microwave radiometers and synthetic aperture radar in remote sensing snow, soil and vegetation, including the development of emission and backscatter models.

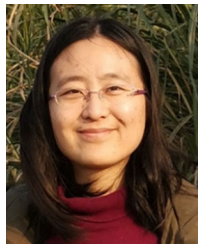

Jinmei Pan received the B.S. and M.S. degrees from the Beijing Normal University, Beijing, China, in 2009 and 2012, respectively, and the Ph.D. degree from the Ohio State University, Columbus, OH, USA, in 2017.

She is currently working with the State Key Laboratory of Remote Sensing Science, Aerospace Information Research Institute, Chinese Academy of Sciences, Beijing, China. She is continuing working on the PM snow depth and SWE retrieval, with snow process models, snow *in-situ* observations in China, snow backscattering observations and modeling, and snowmelt estimation involved.